

Characterization of the numerical group velocity in Yee's FDTD grid

Alvaro Valcarce, *Student Member, IEEE*, Hui Song, *Student Member, IEEE* and Jie Zhang, *Member, IEEE*

Abstract—This paper introduces a method for the optimization of the numerical group velocity \tilde{v}_g in standard finite-difference time-domain (FDTD) electromagnetic simulations. This way, analytical expressions for the extrema of \tilde{v}_g are presented for the first time, thus also characterizing its anisotropy. The knowledge of these expressions is hence essential for the evaluation of the anisotropy error in FDTD-based electrodynamics simulations of the propagation of wavepackets in 2D and 3D. This can be of assistance, for example, in the design of error-bounded FDTD simulations with pulsed sources at low computational cost.

Index Terms—FDTD, group velocity, extrema, anisotropy, wideband, optimization

I. INTRODUCTION

IN recent years, interest has grown in the use of Finite-Difference models for the characterization of large scale radio channels [1] [2] [3]. Furthermore, FDTD simulations have also been used for the study of the propagation conditions of radio communications systems such as ultra-wideband (UWB) [4] [5] [6]. However, the propagation characteristics of wavepackets and that of monochromatic signals in an FDTD grid are fundamentally different. On the one hand single-frequency fields propagate through the grid at a speed given by the numerical phase velocity \tilde{v}_p . On the other hand, the speed of propagation of pulses is governed by the numerical group velocity \tilde{v}_g . Since the dispersion relationship of Yee's grid is not linear, these velocities are not necessarily equal and they vary along different spatial directions. As a consequence of this, numerical electric and magnetic wavepackets propagate with different speeds along different directions. The anisotropy suffered by the numerical phase and group velocities in Yee's FDTD is thus a fundamental source of error in wideband computational electromagnetic simulations.

The extrema of the numerical phase velocity \tilde{v}_p were found by Zhao [7] in 2003, thus characterizing its anisotropy. However, the numerical group velocity \tilde{v}_g has received little attention from the community. The quantification of the anisotropy error suffered by \tilde{v}_g is an essential tool for the evaluation of the accuracy with which the time of arrival (ToA) of wavepackets is predicted in pulsed-source simulations done with FDTD. It is hence a fundamental metric of the accuracy of wideband FDTD simulations such as those presented in [8], which attempt to predict the channel impulse response (CIR) of wireless channels.

In order to quantify the distortion in the propagation of wavepackets due to the anisotropy of \tilde{v}_g , the relative error of

the anisotropy of the numerical group velocity can be defined as

$$\Delta\tilde{v}_{g_{aniso}} = \frac{\hat{v}_M - \hat{v}_m}{\hat{v}_m} \quad (1)$$

where $\hat{v}_M = \max\{\tilde{v}_g\}$ and $\hat{v}_m = \min\{\tilde{v}_g\}$. To evaluate this expression, it is thus necessary to obtain first the extrema of \tilde{v}_g . This was attempted in 2007 in the work presented in [9], but the exact maximum was not found. Instead, a conservative upper bound for the group velocity maximum was provided.

A. Contribution

In this paper, the problem of the optimization of \tilde{v}_g is reformulated and the resulting equations solved using the method of Lagrange multipliers. This way, analytical expressions for the minimum and maximum of the numerical group velocity are obtained in 3D and 2D grids of arbitrary cell sizes. Based on this, (1) can be fully characterized, thus assessing the errors to which the propagation of numerical wavepackets in staggered FDTD grids are subject to.

II. EXTREMA OF NUMERICAL GROUP VELOCITY IN 3D

A. Fundamentals

Let Δx , Δy and Δz be the cell sizes along the x , y and z dimensions in a 3D staggered Yee grid, and let the cell aspect ratios be

$$R_y = \frac{\Delta x}{\Delta y} \quad (2)$$

$$R_z = \frac{\Delta x}{\Delta z}. \quad (3)$$

Further, the numerical dispersion relationship [10] is

$$\frac{1}{(\Delta x)^2} \sin^2 \left(\frac{\tilde{k}_x \Delta x}{2} \right) + \frac{1}{(\Delta y)^2} \sin^2 \left(\frac{\tilde{k}_y \Delta y}{2} \right) + \frac{1}{(\Delta z)^2} \sin^2 \left(\frac{\tilde{k}_z \Delta z}{2} \right) = \frac{1}{(c\Delta t)^2} \sin^2 \left(\frac{\omega \Delta t}{2} \right) \quad (4)$$

where c is the speed of light in the medium being modelled, Δt the time step and ω the angular frequency. Let also ϕ and θ be respectively the azimuth and elevation angles of the propagation direction. Then the Cartesian projections (\tilde{k}_x , \tilde{k}_y and \tilde{k}_z) of the numerical wavevector and its module \tilde{k} are

$$\tilde{k}_x = \tilde{k} \sin(\theta) \cos(\phi) \quad (5)$$

$$\tilde{k}_y = \tilde{k} \sin(\theta) \sin(\phi) \quad (6)$$

$$\tilde{k}_z = \tilde{k} \cos(\theta) \quad (7)$$

The authors are with the Centre for Wireless Network Design (CWIND), Institute for Research on Applicable Computing (IRAC), University of Bedfordshire, Luton, LU1 3JU United Kingdom. e-mail: alvaro.valcarce@beds.ac.uk

$$\tilde{k} = \sqrt{\tilde{k}_x^2 + \tilde{k}_y^2 + \tilde{k}_z^2}. \quad (8)$$

In addition, let also the Courant stability factor be

$$S = \sqrt{\left(\frac{c\Delta t}{\Delta x}\right)^2 + \left(\frac{c\Delta t}{\Delta y}\right)^2 + \left(\frac{c\Delta t}{\Delta z}\right)^2} \quad (9)$$

with $S \in [0, 1]$ for numerical stability. Due to the symmetry of the FDTD grid, the current analysis is presented only in the closed intervals $\phi \in [0, \pi/2]$ and $\theta \in [0, \pi/2]$. The results can thus be extrapolated to other directions by rotating the grid.

B. Optimization

The overall shape of a physical electromagnetic wave moves at the group velocity, which is defined as $v_g \equiv \partial\omega/\partial k$, where k is the angular wavenumber. However in an FDTD grid, the numerical wavenumber \tilde{k} varies with the angular direction, thus causing the anisotropy of the numerical phase and group velocities. Therefore, by clearing ω in the dispersion relationship of (4) and differentiating with respect to \tilde{k} , the numerical group velocity \tilde{v}_g in 3D FDTD can be expressed as

$$\tilde{v}_g = A \cdot \left(\frac{\tilde{k}_x \sin(\tilde{k}_x \Delta x)}{\tilde{k} \Delta x} + \frac{\tilde{k}_y \sin(\tilde{k}_y \Delta y)}{\tilde{k} \Delta y} + \frac{\tilde{k}_z \sin(\tilde{k}_z \Delta z)}{\tilde{k} \Delta z} \right) \quad (10)$$

where the auxiliary variable is

$$A = \frac{c^2}{\omega \text{sinc}(\omega \Delta t)} \quad (11)$$

and $\text{sinc}(x) = \sin(x)/x$ is the unnormalized sinc function.

Theorem 1. *The maximum and minimum values of the numerical group velocity in standard 3D FDTD are*

$$\hat{v}_M = \frac{c}{\cos(\frac{\omega \Delta t}{2})} \sqrt{1 - \frac{1}{S^2} \sin^2\left(\frac{\omega \Delta t}{2}\right)} \quad (12)$$

$$\hat{v}_m = \min_{\zeta \in \{x, y, z\}} \left\{ \frac{c}{\cos(\frac{\omega \Delta t}{2})} \sqrt{1 - \left(\frac{\Delta \zeta}{c \Delta t}\right)^2 \sin^2\left(\frac{\omega \Delta t}{2}\right)} \right\} \quad (13)$$

being the maximum achieved for the propagation direction

$$\phi_{\hat{v}_M} = \arctan(R_y) \quad (14)$$

$$\theta_{\hat{v}_M} = \arctan\left(\frac{\sqrt{1 + R_y^2}}{R_z}\right) \quad (15)$$

and being the minimum achieved for the propagation direction

$$\phi_{\hat{v}_m} = \begin{cases} 0, & \text{if } x = \zeta_{max} \\ \frac{\pi}{2}, & \text{if } y = \zeta_{max} \\ [0, \pi/2], & \text{if } z = \zeta_{max} \end{cases} \quad (16)$$

$$\theta_{\hat{v}_m} = \begin{cases} 0, & \text{if } z = \zeta_{max} \\ \frac{\pi}{2}, & \text{if } x, y = \zeta_{max} \end{cases} \quad (17)$$

where

$$\zeta_{max} = \underset{\zeta \in \{x, y, z\}}{\text{argmax}} \{\Delta \zeta\}. \quad (18)$$

Proof: Finding the extrema of \tilde{v}_g relies on optimizing (10) under the constraint given by (4). Formulating this problem using Lagrange multipliers leads to the following Lagrangian:

$$\begin{aligned} \mathcal{L}_g(\tilde{k}_x, \tilde{k}_y, \tilde{k}_z, \eta_g) = & \frac{\eta_g}{(c\Delta t)^2} \sin^2\left(\frac{\omega \Delta t}{2}\right) + \\ & \left[\frac{A}{\Delta x} \frac{\tilde{k}_x \sin(\tilde{k}_x \Delta x)}{\tilde{k}} - \frac{\eta_g}{(\Delta x)^2} \sin^2\left(\frac{\tilde{k}_x \Delta x}{2}\right) \right] + \\ & \left[\frac{A}{\Delta y} \frac{\tilde{k}_y \sin(\tilde{k}_y \Delta y)}{\tilde{k}} - \frac{\eta_g}{(\Delta y)^2} \sin^2\left(\frac{\tilde{k}_y \Delta y}{2}\right) \right] + \\ & \left[\frac{A}{\Delta z} \frac{\tilde{k}_z \sin(\tilde{k}_z \Delta z)}{\tilde{k}} - \frac{\eta_g}{(\Delta z)^2} \sin^2\left(\frac{\tilde{k}_z \Delta z}{2}\right) \right] \end{aligned} \quad (19)$$

where η_g is a Lagrange multiplier determined by the solution to the system that arises from differentiating (19) and equating to zero. Differentiating (19) with respect to η_g and equating to zero returns the dispersion relationship (4). Then, the other partial derivatives are

$$\begin{aligned} \frac{\partial \mathcal{L}_g}{\partial \tilde{k}_x} = & \frac{A}{\Delta x} \frac{\tilde{k}^2 - \tilde{k}_x^2}{\tilde{k}^3} \sin(\tilde{k}_x \Delta x) + A \frac{\tilde{k}_x}{\tilde{k}} \cos(\tilde{k}_x \Delta x) \\ & - \frac{A}{\Delta y} \frac{\tilde{k}_x \tilde{k}_y}{\tilde{k}^3} \sin(\tilde{k}_y \Delta y) - \frac{A}{\Delta z} \frac{\tilde{k}_x \tilde{k}_z}{\tilde{k}^3} \sin(\tilde{k}_z \Delta z) \\ & - \frac{\eta_g}{2\Delta x} \sin(\tilde{k}_x \Delta x) \end{aligned} \quad (20)$$

$$\begin{aligned} \frac{\partial \mathcal{L}_g}{\partial \tilde{k}_y} = & \frac{A}{\Delta y} \frac{\tilde{k}^2 - \tilde{k}_y^2}{\tilde{k}^3} \sin(\tilde{k}_y \Delta y) + A \frac{\tilde{k}_y}{\tilde{k}} \cos(\tilde{k}_y \Delta y) \\ & - \frac{A}{\Delta x} \frac{\tilde{k}_y \tilde{k}_x}{\tilde{k}^3} \sin(\tilde{k}_x \Delta x) - \frac{A}{\Delta z} \frac{\tilde{k}_y \tilde{k}_z}{\tilde{k}^3} \sin(\tilde{k}_z \Delta z) \\ & - \frac{\eta_g}{2\Delta y} \sin(\tilde{k}_y \Delta y) \end{aligned} \quad (21)$$

$$\begin{aligned} \frac{\partial \mathcal{L}_g}{\partial \tilde{k}_z} = & \frac{A}{\Delta z} \frac{\tilde{k}^2 - \tilde{k}_z^2}{\tilde{k}^3} \sin(\tilde{k}_z \Delta z) + A \frac{\tilde{k}_z}{\tilde{k}} \cos(\tilde{k}_z \Delta z) \\ & - \frac{A}{\Delta x} \frac{\tilde{k}_z \tilde{k}_x}{\tilde{k}^3} \sin(\tilde{k}_x \Delta x) - \frac{A}{\Delta y} \frac{\tilde{k}_z \tilde{k}_y}{\tilde{k}^3} \sin(\tilde{k}_y \Delta y) \\ & - \frac{\eta_g}{2\Delta z} \sin(\tilde{k}_z \Delta z). \end{aligned} \quad (22)$$

In the following analysis, let \tilde{k}_ζ and $\Delta \zeta$ with $\zeta \in \{x, y, z\}$ denote the different components of the wavevector and the spatial steps. Then, by equating (20), (21) and (22) to zero, it can be seen that the extrema of \tilde{v}_g in 3D can occur under three different conditions:

a) Only one \tilde{k}_ζ is nonzero: Let \tilde{k}_ν with $\nu \in \{x, y, z\}$ be the nonzero wavevector component. In this case \tilde{k}_ν is directly obtained from (4). By replacing it in (10), the following extremum of the numerical group velocity is obtained:

$$\tilde{v}_g = \frac{c}{\cos(\frac{\omega \Delta t}{2})} \sqrt{1 - \left(\frac{\Delta \nu}{c \Delta t}\right)^2 \sin^2\left(\frac{\omega \Delta t}{2}\right)}. \quad (23)$$

b) Two \tilde{k}_ζ are nonzero: When only one component of the wavevector is zero, the problem is reduced to one of three possible 2D cases:

- If $\tilde{k}_z = 0$, equations (20), (21) and (22) reduce to

$$\begin{aligned} \frac{\partial \mathcal{L}_g}{\partial \tilde{k}_x} &= \frac{A}{\Delta x} \frac{\tilde{k}^2 - \tilde{k}_x^2}{\tilde{k}^3} \sin(\tilde{k}_x \Delta x) + A \frac{\tilde{k}_x}{\tilde{k}} \cos(\tilde{k}_x \Delta x) \\ &\quad - \frac{A}{\Delta y} \frac{\tilde{k}_x \tilde{k}_y}{\tilde{k}^3} \sin(\tilde{k}_y \Delta y) - \frac{\eta_g}{2\Delta x} \sin(\tilde{k}_x \Delta x) \end{aligned} \quad (24)$$

$$\begin{aligned} \frac{\partial \mathcal{L}_g}{\partial \tilde{k}_y} &= \frac{A}{\Delta y} \frac{\tilde{k}^2 - \tilde{k}_y^2}{\tilde{k}^3} \sin(\tilde{k}_y \Delta y) + A \frac{\tilde{k}_y}{\tilde{k}} \cos(\tilde{k}_y \Delta y) \\ &\quad - \frac{A}{\Delta x} \frac{\tilde{k}_y \tilde{k}_x}{\tilde{k}^3} \sin(\tilde{k}_x \Delta x) - \frac{\eta_g}{2\Delta y} \sin(\tilde{k}_y \Delta y). \end{aligned} \quad (25)$$

This system is solved in Appendix A, where it is seen that the unique solution is $\Delta x \cdot \tilde{k}_x = \Delta y \cdot \tilde{k}_y$, thus leading to the following extremum:

$$\tilde{v}_g = \frac{c}{\cos(\frac{\omega \Delta t}{2})} \sqrt{1 - \left(\frac{\Delta x}{c\Delta t}\right)^2 \frac{1}{1+R_y^2} \sin^2\left(\frac{\omega \Delta t}{2}\right)} \quad (26)$$

- If $\tilde{k}_y = 0$ and following the same 2D approach as in the previous case, the following extremum arises:

$$\tilde{v}_g = \frac{c}{\cos(\frac{\omega \Delta t}{2})} \sqrt{1 - \left(\frac{\Delta x}{c\Delta t}\right)^2 \frac{1}{1+R_z^2} \sin^2\left(\frac{\omega \Delta t}{2}\right)} \quad (27)$$

- Similarly, if $\tilde{k}_x = 0$ then

$$\tilde{v}_g = \frac{c}{\cos(\frac{\omega \Delta t}{2})} \sqrt{1 - \left(\frac{\Delta x}{c\Delta t}\right)^2 \frac{1}{R_y^2 + R_z^2} \sin^2\left(\frac{\omega \Delta t}{2}\right)} \quad (28)$$

c) All \tilde{k}_ζ are nonzero: In this case, the system formed by equaling equations (20), (21) and (22) to zero must be solved, which is done in Appendix B. The unique solution is then found to be $\Delta x \tilde{k}_x = \Delta y \tilde{k}_y = \Delta z \tilde{k}_z$. This implies that this extremum of the numerical group velocity occurs in the same direction as the maximum of the numerical phase velocity (see [7]), being its value

$$\tilde{v}_g = \frac{c}{\cos(\frac{\omega \Delta t}{2})} \sqrt{1 - \frac{1}{S^2} \sin^2\left(\frac{\omega \Delta t}{2}\right)}. \quad (29)$$

Equations (23), (26), (27), (28) and (29) are the extrema of \tilde{v}_g in 3D. However, it still remains to be determined which one is the maximum and which one is the minimum. A comparison is thus made in the following:

a) Comparing (29) with (23): If \tilde{k}_ν is the nonzero component in (23), and S is given by (9), then

$$S^2 > \left(\frac{c\Delta t}{\Delta \nu}\right)^2 \Rightarrow \left(\frac{\Delta \nu}{c\Delta t}\right)^2 > \frac{1}{S^2}. \quad (30)$$

And therefore (29) is larger than (23).

b) Comparing (29) with (26):

$$S^2 > \left(\frac{c\Delta t}{\Delta x}\right)^2 + \left(\frac{c\Delta t}{\Delta y}\right)^2 = \left(\frac{c\Delta t}{\Delta x}\right)^2 \cdot (1 + R_y^2). \quad (31)$$

Hence

$$\left(\frac{\Delta x}{c\Delta t}\right)^2 \cdot \frac{1}{1 + R_y^2} > \frac{1}{S^2}. \quad (32)$$

And thus (29) is larger than (26).

c) Comparing (29) with (27): Applying the same approach as in the previous case, it results that

$$\left(\frac{\Delta x}{c\Delta t}\right)^2 \cdot \frac{1}{1 + R_z^2} > \frac{1}{S^2}. \quad (33)$$

And thus (29) is larger than (27).

d) Comparing (29) with (28): Applying the same approach once again, it results that

$$\left(\frac{\Delta x}{c\Delta t}\right)^2 \cdot \frac{1}{R_y^2 + R_z^2} > \frac{1}{S^2}. \quad (34)$$

And thus (29) is larger than (28).

Since (29) is larger than any of the other extrema in 3D, it is thus clear that (29) is the maximum of the numerical group velocity. Then, the minimum of \tilde{v}_g is determined by the minimum of equations (23), (26), (27) and (28). It then results that the minimum occurs when only one \tilde{k}_ζ is nonzero (i.e. along the axis with largest spatial step). Thus equation (23) is the minimum. Furthermore, since these extrema are achieved for the same \tilde{k}_ζ as the numerical phase velocity, the propagation directions (ϕ, θ) of the extrema are the same as those presented in [7]. ■

Note that, for cubic grid cells $\zeta_{max} = x, y, z$ and so the minimum is achieved $\forall \phi \in [0, \pi/2]$ when $\theta = 0$ and also for $\phi = 0$ and $\phi = \pi/2$ when $\theta = \pi/2$. On the other hand, the maximum occurs only for the propagation direction $(\phi, \theta) = (\pi/4, \arctan(\sqrt{2}))$.

III. EXTREMA OF NUMERICAL GROUP VELOCITY IN 2D

A. Fundamentals

The equation for the numerical dispersion in 2D is

$$\begin{aligned} \frac{1}{(\Delta x)^2} \sin^2\left(\frac{\tilde{k}_x \Delta x}{2}\right) + \frac{1}{(\Delta y)^2} \sin^2\left(\frac{\tilde{k}_y \Delta y}{2}\right) \\ = \frac{1}{(c\Delta t)^2} \sin^2\left(\frac{\omega \Delta t}{2}\right) \end{aligned} \quad (35)$$

and the Cartesian projections of the numerical wavevector and its module \tilde{k} are

$$\tilde{k}_x = \tilde{k} \cos(\phi) \quad (36)$$

$$\tilde{k}_y = \tilde{k} \sin(\phi) \quad (37)$$

$$\tilde{k} = \sqrt{\tilde{k}_x^2 + \tilde{k}_y^2} \quad (38)$$

with ϕ the propagation angle with respect to the positive x direction. Similarly, the 2D Courant stability factor is

$$S = \sqrt{\left(\frac{c\Delta t}{\Delta x}\right)^2 + \left(\frac{c\Delta t}{\Delta y}\right)^2} \quad (39)$$

with $S \in [0, 1]$ for numerical stability.

B. Optimization

The expression for the numerical group velocity in 2D is

$$\tilde{v}_g = A \cdot \left(\frac{\tilde{k}_x \sin(\tilde{k}_x \Delta x)}{\tilde{k} \Delta x} + \frac{\tilde{k}_y \sin(\tilde{k}_y \Delta y)}{\tilde{k} \Delta y} \right). \quad (40)$$

As seen in the following, the optimization process in 2D results from a simplified 3D case.

Theorem 2. *The maximum and minimum values of the numerical group velocity in standard 2D FDTD are*

$$\hat{v}_M = \frac{c}{\cos(\frac{\omega \Delta t}{2})} \sqrt{1 - \frac{1}{S^2} \sin^2(\frac{\omega \Delta t}{2})} \quad (41)$$

$$\hat{v}_m = \min_{\zeta \in \{x, y\}} \left\{ \frac{c}{\cos(\frac{\omega \Delta t}{2})} \sqrt{1 - \left(\frac{\Delta \zeta}{c \Delta t} \right)^2 \sin^2(\frac{\omega \Delta t}{2})} \right\} \quad (42)$$

which are achieved respectively for the propagation directions

$$\phi_{\hat{v}_M} = \arctan(R_y) \quad (43)$$

$$\phi_{\hat{v}_m} = \begin{cases} 0, & \text{if } R_y \geq 1 \\ \frac{\pi}{2}, & \text{if } R_y \leq 1 \end{cases} \quad (44)$$

Proof: Similarly to the 3D case, the Lagrangian is

$$\mathcal{L}_g(\tilde{k}_x, \tilde{k}_y, \eta_g) = \frac{\eta_g}{(c \Delta t)^2} \sin^2\left(\frac{\omega \Delta t}{2}\right) + \left[\frac{A}{\Delta x} \frac{\tilde{k}_x \sin(\tilde{k}_x \Delta x)}{\tilde{k}} - \frac{\eta_g}{(\Delta x)^2} \sin^2\left(\frac{\tilde{k}_x \Delta x}{2}\right) \right] + \left[\frac{A}{\Delta y} \frac{\tilde{k}_y \sin(\tilde{k}_y \Delta y)}{\tilde{k}} - \frac{\eta_g}{(\Delta y)^2} \sin^2\left(\frac{\tilde{k}_y \Delta y}{2}\right) \right] \quad (45)$$

The derivatives with respect to \tilde{k}_x and \tilde{k}_y in this case are those shown in equations (24) and (25). In the following and just as in the 3D case, let \tilde{k}_ζ and $\Delta \zeta$ with $\zeta \in \{x, y\}$ denote the different components of the wavevector and the spatial steps. Then, this system of equations has solutions under two different conditions:

1) *Only one \tilde{k}_ζ is nonzero:* In this case, let \tilde{k}_ν with $\nu \in \{x, y\}$ be the nonzero component of the wavevector, which can be directly obtained from the 2D dispersion relationship. Then, by plugging it into (40), this extremum of the numerical group velocity is the one shown in equation (23).

2) *All \tilde{k}_ζ are nonzero:* In this case, the system formed by equaling (24) and (25) to zero must be solved. This is done in Appendix A, where it is seen that the unique solution is $\Delta x \cdot \tilde{k}_x = \Delta y \cdot \tilde{k}_y$, thus leading to the value of the numerical group velocity shown in equation (29).

The results of (23) and (29) identify the extrema of \tilde{v}_g in 2D. Then, in order to find out whether these are maximums or minimums, they must be compared. From (39), it is clear that equation (30) holds $\forall \nu \in \{x, y\}$, in view of which, (29) is the maximum of the numerical group velocity and (23) is the minimum. Furthermore, these values are achieved for the same \tilde{k}_ζ as the numerical phase velocity (see [7] and [9]) and thus also for the same propagation angle ϕ . ■

Also note that, for square grid cells, the minimum of the numerical group velocity is achieved at both angles 0 and $\pi/2$. On the other hand the maximum occurs only at $\phi = \pi/4$.

TABLE I
THEORETICAL \tilde{v}_g EXTREMA IN 3D FDTD

R_y	R_z	S	N_λ	\hat{v}_m/c	\hat{v}_M/c	$\Delta \tilde{v}_{g_{aniso}}$ [%]
1	1	1	20	0.9917	1	0.837
			10	0.9658	1	3.543
		0.5	20	0.9886	0.9969	0.839
			10	0.9534	0.9875	3.575
2	3	1	20	0.9885	1	1.167
			10	0.9529	1	4.948
		0.5	20	0.9878	0.9993	1.168
			10	0.9502	0.9974	4.958

IV. NUMERICAL VALIDATION

The solution \tilde{k} of the numerical dispersion relationship can be approximated with numerical analysis (e.g. using the Newton-Raphson method). Then, by substituting the obtained \tilde{k} into (10) for 3D or into (40) for 2D, a good approximation to \tilde{v}_g can be computed. Next, the theoretical extrema of \tilde{v}_g obtained in the previous sections are validated. This is done by showing that the numerically computed \tilde{v}_g is always bounded by these theoretical extrema. Furthermore, it can be experimentally observed that the higher the accuracy with which \tilde{k} is resolved, the closer the numerically obtained extrema of \tilde{v}_g will be to the predicted theoretical values.

In the 3D case, Figures 1 and 2 show numerically computed values of \tilde{v}_g for different grid parameters, as well as the theoretical extrema according to Theorem 1. The angle resolution is $\Delta \phi = 0.09^\circ$ and \tilde{k} is approximated using the Newton-Raphson method with an accuracy of 10^{-9} . In these examples $R_y \geq 1$, $R_z \geq 1$ and without loss of generality the grid resolution is defined as $N_\lambda = \lambda/\Delta x$, where λ is the physical dominant wavelength. Also for convenience, the sine argument $\omega \Delta t/2$ is expressed in terms of the FDTD grid parameters:

$$\frac{\omega \Delta t}{2} = \frac{2\pi c \Delta t}{2\lambda} = \frac{\pi}{N_\lambda} \frac{c \Delta t}{\Delta x} = \frac{\pi}{N_\lambda} \cdot \frac{S}{\sqrt{1 + R_y^2 + R_z^2}} \quad (46)$$

This highlights that the extrema of \tilde{v}_g and its anisotropy error in 3D depend mainly on R_y , R_z , S , and N_λ . Table I illustrates the theoretical values of the anisotropy error $\Delta \tilde{v}_{g_{aniso}}$ and the extrema. It can be seen that these match well the numerical results on Figures 1 and 2. The dependence of $\phi_{\hat{v}_M}$ with the cells aspect ratios is further illustrated in Figure 2, where non-cubic cells are used. In addition, the anisotropy error in 3D and its dependence with the grid resolution is also illustrated in Figure 3(a). Finally and to give a global and clearer geometrical view of the behavior of \tilde{v}_g , Figure 4 shows the numerically computed normalized group velocity values for a wider range of angular directions in the case of cubic cells with angle resolutions $\Delta \phi = 0.09^\circ$ and $\Delta \theta = 0.09^\circ$.

For the 2D case, Figure 5 shows numerically computed values of the normalized numerical group velocity \tilde{v}_g/c in relationship with the propagation angle ϕ . For comparison purposes, the theoretical extrema of \tilde{v}_g/c according to Theorem 2 are also plotted in this Figure. The angle resolution is $\Delta \phi = 0.09^\circ$ and \tilde{k} is approximated using the Newton-Raphson method with an accuracy of 10^{-9} . Also, $R_y \geq 1$ and again

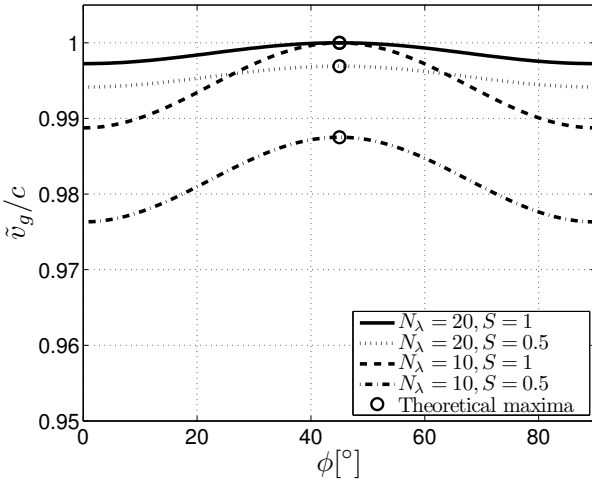
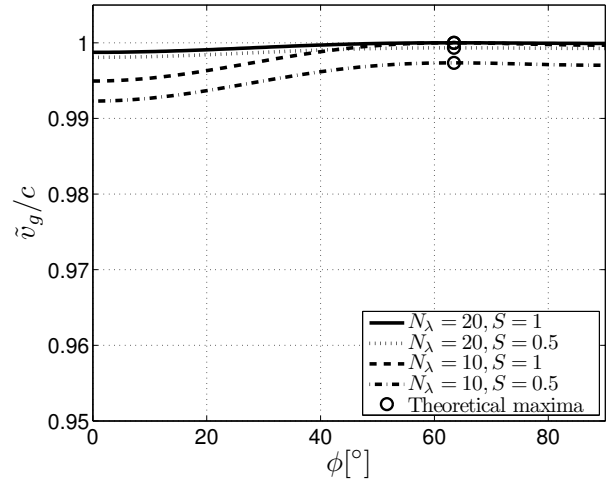
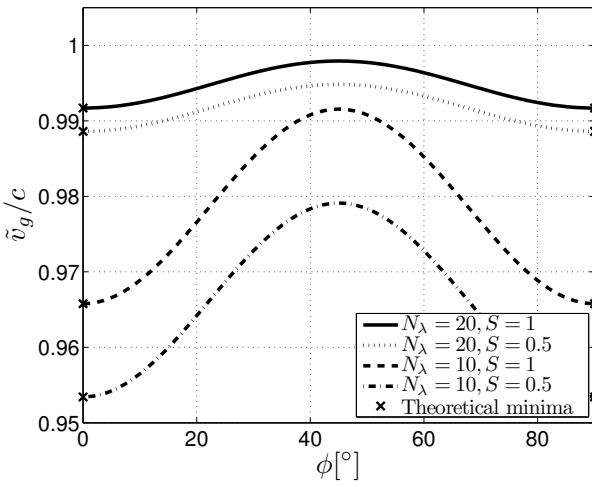
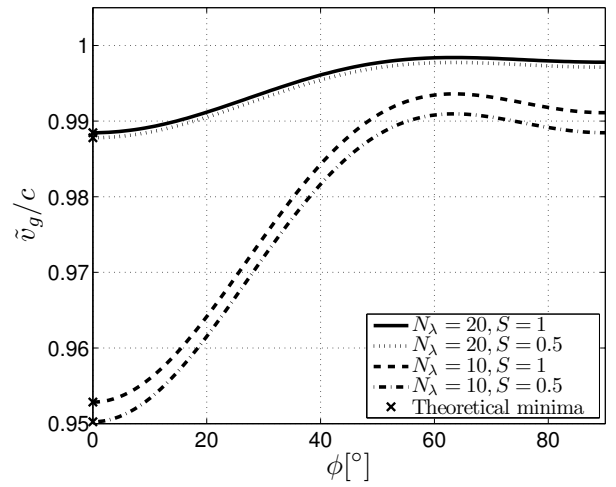
(a) $\theta = \arctan(\sqrt{1+R_y^2}/R_z)$ (a) $\theta = \arctan(\sqrt{1+R_y^2}/R_z)$ (b) $\theta = 90^\circ$ (b) $\theta = 90^\circ$

Fig. 1. Normalized numerical group velocity in 3D FDTD with $N_\lambda = \lambda/\Delta x$, $R_y = 1$ and $R_z = 1$.

Fig. 2. Normalized numerical group velocity in 3D FDTD with $N_\lambda = \lambda/\Delta x$, $R_y = 2$ and $R_z = 3$.

without loss of generality the grid resolution is $N_\lambda = \lambda/\Delta x$. This way, the sine argument $\omega\Delta t/2$ can be expressed as

$$\frac{\omega\Delta t}{2} = \frac{\pi}{N_\lambda} \cdot \frac{S}{\sqrt{1+R_y^2}} \quad (47)$$

to highlight the main parameters that influence the anisotropy of \tilde{v}_g . In addition, Table II contains the theoretical values of the extrema and of the anisotropy error. Then, simple visual inspection of Figure 5 and Table II reveals that the numerical results agree with the presented theory. This Figure also illustrates the dependency of $\phi_{\tilde{v}_M}$ with the cell aspect ratio R_y (see equation (43)) and, finally, the dependence of the anisotropy error with the grid resolution in 2D is illustrated in Figure 3(b).

V. CONCLUSIONS

Conclusion 1: The current paper has obtained analytical expressions for the extrema of the numerical group velocity in 3D and 2D FDTD grids of arbitrary cell sizes. In view of

TABLE II
THEORETICAL \tilde{v}_g EXTREMA IN 2D FDTD

R_y	S	N_λ	\hat{v}_m/c	\hat{v}_M/c	$\Delta\tilde{v}_{g_{aniso}}$ [%]
1	1	20	0.9938	1	0.628
		10	0.9742	1	2.653
	0.5	20	0.9891	0.9954	0.628
		10	0.9555	0.9812	2.653
1.5	1	20	0.9914	1	0.870
		10	0.9645	1	3.680
	0.5	20	0.9885	0.9972	0.870
		10	0.9531	0.9885	3.711

equation (1), these results also characterize fully the anisotropy error of the numerical group velocity.

Conclusion 2: Furthermore, equations (58) and (68) have shown that the numerical group velocity achieves its maximum along the same propagation direction as the maximum of the numerical phase velocity \tilde{v}_p (see [7]).

Conclusion 3: Equations (12) and (41) also reveal that \tilde{v}_g can be faster than c (faster-than-light or superluminal numerical pulse propagation) when $S > 1$. However, such

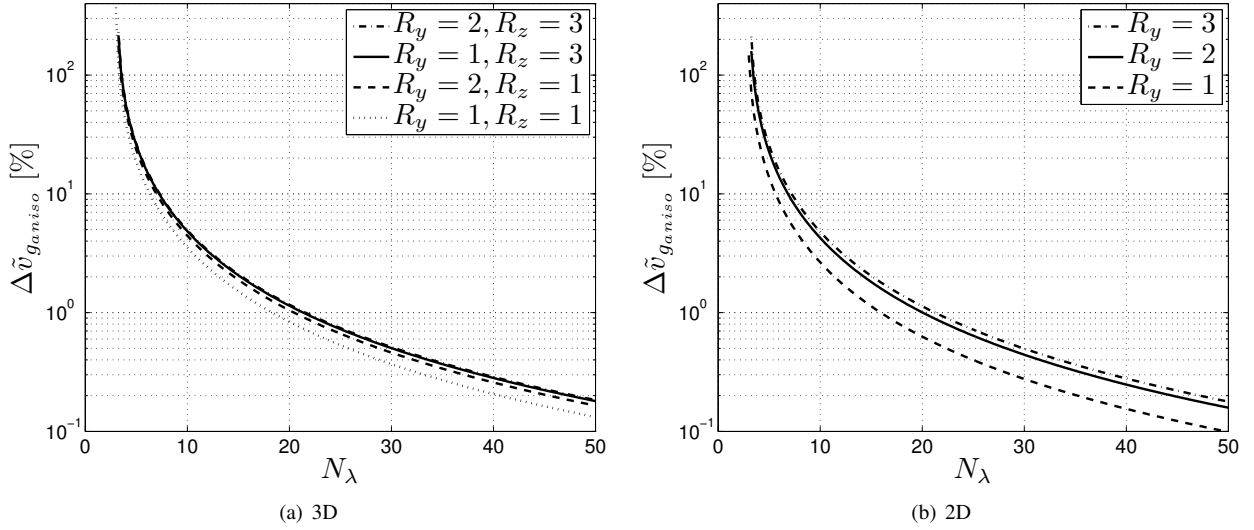


Fig. 3. Anisotropy error of the numerical group velocity when $S = 1$ and calculated with the theoretical formulas introduced in Theorems 1 and 2.

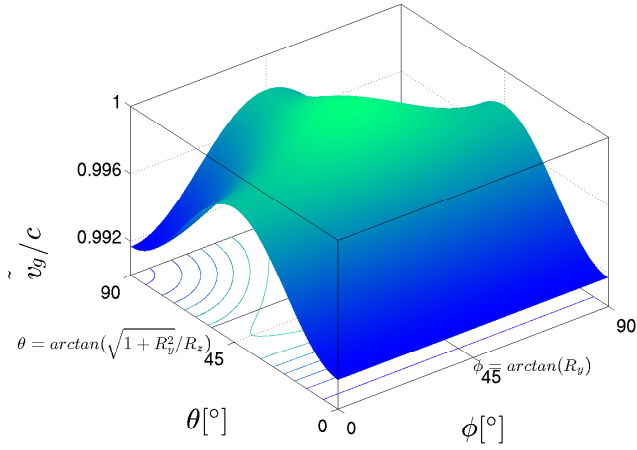
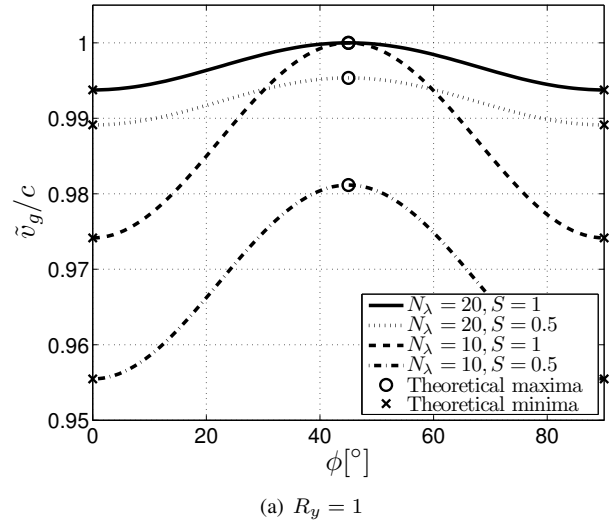
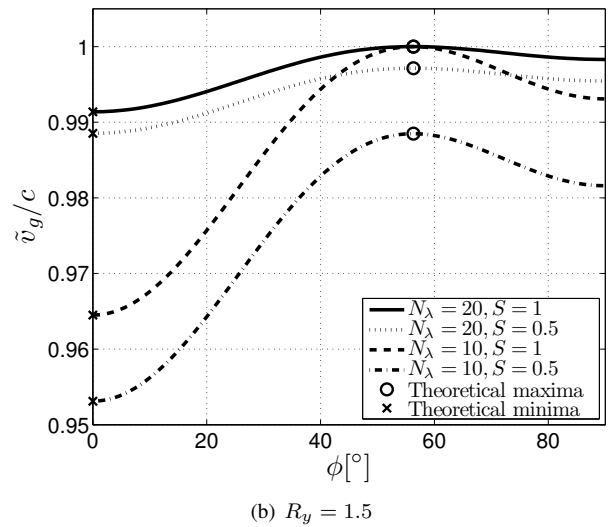


Fig. 4. Normalized numerical group velocity in 3D FDTD with $N_\lambda = \lambda/\Delta x = 20$, $S = 1$ and $R_y = 1$ and $R_z = 1$.



(a) $R_y = 1$



(b) $R_y = 1.5$

Fig. 5. Normalized numerical group velocity in 2D FDTD with $N_\lambda = \lambda/\Delta x$.

solutions are known to be numerically unstable [10].

Conclusion 4: From (41) and (12), it can also be seen that $\hat{v}_M = c$ when $S = 1$. Therefore in this case, the anisotropy error is fully defined by the equations of \hat{v}_m .

Conclusion 5: The extrema of \tilde{v}_g reveal that the anisotropy error depends not only on the grid properties but also on the speed of propagation c in the medium being modelled. Thus, if simulations containing different non-lossy media are considered, $\Delta \tilde{v}_{g_{aniso}}$ will be larger within those materials with a lower propagation speed (i.e. with a higher refractive index). Nevertheless, the general formulation of the equations provided by Theorems 1 and 2 can be applied to predict the anisotropy error in any non-lossy media involved in the simulation, given that the value of c for each material is known. The grid parameters can then be adjusted to guarantee a maximum anisotropy error in the medium with the lowest propagation speed.

To sum up, this paper has rigorously shown the geometrical behavior of the numerical group velocity in FDTD Yee grids

of arbitrary cell aspect ratios. Since the extrema of \tilde{v}_g occur along the same direction as the extrema of \tilde{v}_p , the term *special direction* used by Zhao [7] acquires higher significance. In general terms, the current work establishes a solid framework for the accuracy evaluation of FDTD algorithms that deal with the transmission of wavepackets. This can include, for instance, assessments of the anisotropy error of FDTD-based radio channel estimations (e.g. CIR simulations) as well as UWB.

ACKNOWLEDGMENT

This work is supported by the EU FP6 RANPLAN-HEC project on *Automatic 3G/4G Radio Access Network Planning and Optimisation - A High End Computing Approach* under grant number MC-EST-2005-020958.

APPENDIX A

The system that arises from equating (24) and (25) to zero can be rewritten as

$$\begin{aligned} \frac{\tilde{k}_x^2 - k_x^2}{\tilde{k}_x^3} + \frac{\tilde{k}_x \Delta x}{k \cdot \tan(\tilde{k}_x \Delta x)} - \frac{\Delta x}{\Delta y} \frac{\tilde{k}_x \tilde{k}_y}{\tilde{k}_x^3} \frac{\sin(\tilde{k}_y \Delta y)}{\sin(\tilde{k}_x \Delta x)} &= \frac{\eta_g}{2A} \\ \frac{\tilde{k}_y^2 - k_y^2}{\tilde{k}_y^3} + \frac{\tilde{k}_y \Delta y}{k \cdot \tan(\tilde{k}_y \Delta y)} - \frac{\Delta y}{\Delta x} \frac{\tilde{k}_x \tilde{k}_y}{\tilde{k}_y^3} \frac{\sin(\tilde{k}_x \Delta x)}{\sin(\tilde{k}_y \Delta y)} &= \frac{\eta_g}{2A}. \end{aligned} \quad (48)$$

For simplification, the following variables are defined:

$$\begin{aligned} \sigma_x &= \Delta x \cdot \tilde{k}_x \\ \sigma_y &= \Delta y \cdot \tilde{k}_y \\ \alpha &= \Delta x \cdot \tilde{k} \\ \beta &= \Delta y \cdot \tilde{k}. \end{aligned} \quad (49)$$

which are all strictly positive. Furthermore, Yee grids have at least two cells per wavelength and therefore

$$|\tilde{k}_\zeta \Delta \zeta| \leq \pi \quad \forall \zeta \in \{x, y\}. \quad (50)$$

Hence $\sigma_x, \sigma_y \in (0, \pi]$. Then, equating the left hand side terms in the equations of (48) gives rise to the following equation:

$$\Gamma = 0 \quad (51)$$

where $\Gamma = \Psi_1 + \Psi_2 + \Psi_3$ and the auxiliary variables are

$$\Psi_1 = \frac{\sigma_y}{\tan(\sigma_y)} - \frac{\sigma_x}{\tan(\sigma_x)} \quad (52)$$

$$\Psi_2 = \left(\frac{\sigma_x}{\alpha} \right)^2 - \frac{\sigma_x \sigma_y}{\alpha^2} \frac{\sin(\sigma_x)}{\sin(\sigma_y)} \quad (53)$$

$$\Psi_3 = \frac{\sigma_x \sigma_y}{\beta^2} \frac{\sin(\sigma_y)}{\sin(\sigma_x)} - \left(\frac{\sigma_y}{\beta} \right)^2. \quad (54)$$

It can be easily tested that $\sigma_x = \sigma_y$ is a solution of (51). Therefore it is necessary to test whether this is the only solution or not. This is done in the following by studying the sign of Γ :

a) *Case $\sigma_x > \sigma_y$* : Let us first analyse Ψ_1 . Since $x/\tan(x)$ is a monotonically decreasing function, $\sigma_x > \sigma_y$ yields $\Psi_1 > 0$.

Let us now look into Ψ_2 . Equation (53) can be rewritten as

$$\Psi_2 = \frac{\sigma_x}{\alpha^2 \sin(\sigma_y)} (\sigma_x \cdot \sin(\sigma_y) - \sigma_y \cdot \sin(\sigma_x)) \quad (55)$$

and it can then be seen that the sign of Ψ_2 only depends on the terms in parenthesis, since $\sigma_x/(\alpha^2 \sin(\sigma_y))$ is strictly positive in the interval under consideration. To analyse this, consider the following function:

$$F = \frac{\sigma_x \cdot \sin(\sigma_y)}{\sigma_y \cdot \sin(\sigma_x)} = \frac{\text{sinc}(\sigma_y)}{\text{sinc}(\sigma_x)}. \quad (56)$$

Since $\text{sinc}(x)$ is monotonically decreasing in $(0, \pi]$, it is clear that $F > 1$ when $\sigma_x > \sigma_y$ and thus $\sigma_x \cdot \sin(\sigma_y) > \sigma_y \cdot \sin(\sigma_x)$. Hence $\Psi_2 > 0$ for $\sigma_x > \sigma_y$.

In a similar way, Ψ_3 can be rewritten as

$$\Psi_3 = \frac{\sigma_y}{\beta^2 \sin(\sigma_x)} (\sigma_x \cdot \sin(\sigma_y) - \sigma_y \cdot \sin(\sigma_x)). \quad (57)$$

Using the previous result, it turns out that $\Psi_3 > 0$ when $\sigma_x > \sigma_y$.

Therefore, $\Gamma > 0$ when $\sigma_x > \sigma_y$.

b) *Case $\sigma_x < \sigma_y$* : Using the results from the previous case, it is straightforward to prove that $\Psi_1 < 0$, $\Psi_2 < 0$ and $\Psi_3 < 0$ when $\sigma_x < \sigma_y$. Therefore $\Gamma < 0$ in this case.

c) *Case $\sigma_x = \sigma_y$* : In this case, $\Gamma = 0$.

Thus, the sign of Γ is constant when $\sigma_x > \sigma_y$ and $\sigma_x < \sigma_y$. Furthermore, Γ is a continuous function in the domains of σ_x and σ_y . Therefore, $\sigma_x = \sigma_y$ is the only solution of (51), which yields

$$\Delta x \cdot \tilde{k}_x = \Delta y \cdot \tilde{k}_y. \quad (58)$$

APPENDIX B

By equating to zero equations (20), (21) and (22), the following system of equations arises:

$$\begin{aligned} \frac{\tilde{k}_x^2 - k_x^2}{\tilde{k}_x^3} + \frac{\tilde{k}_x \Delta x}{k \cdot \tan(\tilde{k}_x \Delta x)} - \frac{\Delta x}{\Delta y} \frac{\tilde{k}_x \tilde{k}_y}{\tilde{k}_x^3} \frac{\sin(\tilde{k}_y \Delta y)}{\sin(\tilde{k}_x \Delta x)} &= \frac{\eta_g}{2A} \\ - \frac{\Delta x}{\Delta z} \frac{\tilde{k}_x \tilde{k}_z}{\tilde{k}_x^3} \frac{\sin(\tilde{k}_z \Delta z)}{\tilde{k}_x \Delta x} &= \frac{\eta_g}{2A} \\ \frac{\tilde{k}_y^2 - k_y^2}{\tilde{k}_y^3} + \frac{\tilde{k}_y \Delta y}{k \cdot \tan(\tilde{k}_y \Delta y)} - \frac{\Delta y}{\Delta x} \frac{\tilde{k}_y \tilde{k}_x}{\tilde{k}_y^3} \frac{\sin(\tilde{k}_x \Delta x)}{\sin(\tilde{k}_y \Delta y)} &= \frac{\eta_g}{2A} \\ - \frac{\Delta y}{\Delta z} \frac{\tilde{k}_y \tilde{k}_z}{\tilde{k}_y^3} \frac{\sin(\tilde{k}_z \Delta z)}{\sin(\tilde{k}_y \Delta y)} &= \frac{\eta_g}{2A} \\ \frac{\tilde{k}_z^2 - k_z^2}{\tilde{k}_z^3} + \frac{\tilde{k}_z \Delta z}{k \cdot \tan(\tilde{k}_z \Delta z)} - \frac{\Delta z}{\Delta x} \frac{\tilde{k}_z \tilde{k}_x}{\tilde{k}_z^3} \frac{\sin(\tilde{k}_x \Delta x)}{\sin(\tilde{k}_z \Delta z)} &= \frac{\eta_g}{2A} \\ - \frac{\Delta z}{\Delta y} \frac{\tilde{k}_z \tilde{k}_y}{\tilde{k}_z^3} \frac{\sin(\tilde{k}_y \Delta y)}{\sin(\tilde{k}_z \Delta z)} &= \frac{\eta_g}{2A}. \end{aligned} \quad (59)$$

To simplify the notation, the following variables are defined in addition to those of (49):

$$\begin{aligned} \sigma_z &= \Delta z \cdot \tilde{k}_z \\ \gamma &= \Delta z \cdot \tilde{k}. \end{aligned} \quad (60)$$

Then, by equating the terms in the left hand side of (59) the following equations are obtained:

$$\Psi_1 + \Psi_2 + \Psi_3 + \Psi_4 = 0 \quad (61)$$

$$\Psi_5 + \Psi_6 + \Psi_7 + \Psi_8 = 0 \quad (62)$$

where the additional auxiliary variables are

$$\Psi_4 = \frac{\sigma_z \sin(\sigma_z)}{\gamma^2} \cdot \left(\frac{\sigma_x}{\sin(\sigma_x)} - \frac{\sigma_y}{\sin(\sigma_y)} \right) \quad (63)$$

$$\Psi_5 = \frac{\sigma_y}{\tan(\sigma_y)} - \frac{\sigma_z}{\tan(\sigma_z)} \quad (64)$$

$$\Psi_6 = \left(\frac{\sigma_z}{\gamma} \right)^2 - \frac{\sigma_y \sigma_z \sin(\sigma_z)}{\gamma^2 \sin(\sigma_y)} \quad (65)$$

$$\Psi_7 = \frac{\sigma_z \sigma_y \sin(\sigma_y)}{\beta^2 \sin(\sigma_z)} - \left(\frac{\sigma_y}{\beta} \right)^2 \quad (66)$$

$$\Psi_8 = \frac{\sigma_x \sin(\sigma_x)}{\alpha^2} \cdot \left(\frac{\sigma_z}{\sin(\sigma_z)} - \frac{\sigma_y}{\sin(\sigma_y)} \right). \quad (67)$$

Applying a similar analysis as in Appendix A, it is easy to see that $\Psi_4 = 0$ only when $\sigma_x = \sigma_y$. Furthermore, $\Psi_4 > 0$ when $\sigma_x > \sigma_y$, and $\Psi_4 < 0$ when $\sigma_x < \sigma_y$, thus denoting $\sigma_x = \sigma_y$ as the only solution of (61). Similarly $\Psi_8 = 0$ only if $\sigma_y = \sigma_z$, $\Psi_8 > 0$ when $\sigma_y > \sigma_z$, and $\Psi_8 < 0$ when $\sigma_y < \sigma_z$. Equations (64), (65) and (66) have respectively the same form as (52), (53) and (54) and hence their analysis is equivalent. As a consequence of this, the unique solution of (59) is

$$\Delta x \tilde{k}_x = \Delta y \tilde{k}_y = \Delta z \tilde{k}_z. \quad (68)$$

REFERENCES

- [1] G. Rodriguez, Y. Miyazaki, and N. Goto, "Matrix-Based FDTD Parallel Algorithm for Big Areas and Its Applications to High-Speed Wireless Communications," *IEEE Transactions on Antennas and Propagation*, vol. 54, pp. 785–796, March 2006.
- [2] A. Alighanbari and C. D. Sarris, "Rigorous and Efficient Time-Domain Modeling of Electromagnetic Wave Propagation and Fading Statistics in Indoor Wireless Channels," *IEEE Transactions on Antennas and Propagation*, vol. 55, no. 8, pp. 2373–2381, Aug. 2007.
- [3] M. Thiel and K. Sarabandi, "A Hybrid Method for Indoor Wave Propagation Modeling," *IEEE Transactions on Antennas and Propagation*, vol. 56, no. 8, pp. 2703–2709, Aug. 2008.
- [4] Y. Zhao, Y. Hao, A. Alomainy, and C. Parini, "UWB On-Body Radio Channel Modelling Using Ray Theory and Sub-band FDTD Method," *IEEE Transactions on Microwave Theory and Techniques*, vol. 54, no. 4, pp. 1827–1835, Jun. 2006.
- [5] A. Thiry, F. Costen, and A. Brown, "Numerical noise introduced by the alternating direction-implicit scheme in FDTD for UWB systems," *International Journal on Wireless & Optical Communications (IJWOC)*, vol. 3, no. 2, pp. 135–143, 2006.
- [6] Y. Zhao, Y. Hao, and C. Parini, "FDTD characterisation of UWB indoor radio channel including frequency dependent antenna directivities," *IEEE Antennas and Wireless Propagation Letters*, vol. 6, pp. 191–194, 2007.
- [7] A. P. Zhao, "Determination of the Direction That Has Maximum Phase-Velocity for the 2-D and 3-D FDTD Methods Based on Yee's Algorithm," *IEEE Microwave and Wireless Components Letters*, vol. 13, no. 6, pp. 226–228, Jun. 2003.
- [8] A. Alighanbari and C. D. Sarris, "Parallel Time-Domain Full-Wave Analysis and System-Level Modeling of Ultrawideband Indoor Communication Systems," *IEEE Transactions on Antennas and Propagation*, vol. 57, no. 1, pp. 231–240, Jan. 2009.
- [9] M. Premaratne and S. K. Halgamuge, "Rigorous Analysis of Numerical Phase and Group Velocity Bounds in Yee's FDTD Grid," *IEEE Microwave and wireless components letters*, vol. 17, no. 8, pp. 556–558, Aug. 2007.
- [10] A. Taflov and S. C. Hagness, *Computational Electrodynamics: The Finite-Difference Time-Domain Method*, 3rd ed. Artech House, 2005.



Alvaro Valcarce received his M.Eng. in Telecommunications Engineering from the University of Vigo (Spain) in 2006. Between 2006 and 2007 he worked at the WiSAAR consortium in Saarbrücken (Germany), performing WiMAX field trials and analysing radio coverage measurements. He joined the Centre for Wireless Network Design (CWIND) at the University of Bedfordshire (U.K.) in 2007 with the support of a European Marie Curie Fellowship for Early Stage Researchers. Since then, he has been involved in feasibility studies of OFDMA femtocells

for indoor coverage, with special interest in interference avoidance for WiMAX and LTE femtocells. His work included the design and evaluation of algorithms for the distributed allocation of OFDMA resources, as well as the analysis of hybrid access policies in two-tier networks. At the same time, Alvaro has done research in the field of computational electrodynamics, being this the central topic of his doctoral studies. He is interested in studying techniques that facilitate the application of numerical solutions to large-scale electromagnetic problems (indoor and outdoor environments for wireless communications). Currently, he is investigating the errors that arise when Yee's FDTD algorithm is used for performing channel impulse response simulations with small grid resolutions.



Hui Song received his B.A.Sc in Mathematics from Fudan University, China in 2005. From 2004 to 2006, he worked for Bynear Telesoft as an R&D engineer on network planning and optimization techniques (including GSM, WCDMA and TD-SCDMA) in Shanghai, China. Since 2006, he has been a Marie Curie research associate at the Center for Wireless Network Design (CWIND), University of Bedfordshire. He obtained his Ph.D in wireless communications at University of Bedfordshire in 2010. His current research interests are in the area of

link adaptation and channel modeling for MIMO-OFDMA systems. Further, he is a contributor of the book "Femtocell: Technologies and Deployment" (Wiley, 2010).



Jie Zhang is a Professor of Wireless Communications and Networks at the Department of Computer Science and Technology, University of Bedfordshire. He received his PhD in Industrial Automation from the East China University of Science and Technology in 1995. From 1997 to 2001, he was a research fellow with University College London, Imperial College London and Oxford University. He is the founding director of CWIND, one of the largest and leading research groups in 3G/4G radio access network planning and optimization in Europe.

CWiND is a world leader in indoor wireless network design and femtocell research. Since 2003, as the Principal Investigator, he has been awarded 17 projects worth some US\$10 million (his share) by the EPSRC, the European Commission (FP6/FP7), the industry, etc. He is a Co-Investigator of two EPSRC-funded projects on femtocells and 4G/B4G mobile communications. His main research interests include radio propagation, 3G/4G network simulation, planning and optimization, self-organizing networks (SON), indoor wireless network design and femtocells. He is an Associate Editor of Telecommunications Systems (Springer) and an Area Editor of Computer Communications (Elsevier). He has published over 100 refereed journal and conference papers and is a lead author of the book Femtocells: Technologies and Deployment (Wiley, Jan. 2010).